Essential Role of XBP1 in Maintaining Photoreceptor Synaptic Integrity in Early Diabetic Retinopathy

Todd McLaughlin,[1] Grant Wang,[1] Andy Medina,[1] Jacob Perkins,[1] Rhudwan Nihlawi,[1] Don Seyfried,[1] Zihua Hu,[1,2] Joshua J. Wang,[1,3] and Sarah X. Zhang[1,3]

[1]Department of Ophthalmology and Ross Eye Institute, University at Buffalo, State University of New York, Buffalo, New York, United States
[2]Center for Computational Research, New York State Center of Excellence in Bioinformatics and Life Sciences, State University of New York, Buffalo, New York, United States
[3]Department of Biochemistry, State University of New York, Buffalo, New York, United States

Correspondence: Sarah X. Zhang, 955 Main Street, JSMBS, Buffalo, NY 14203, USA;
xzhang38@buffalo.edu.

Received: September 22, 2023
Accepted: November 4, 2023
Published: November 28, 2023

Citation: McLaughlin T, Wang G, Medina A, et al. Essential role of XBP1 in maintaining photoreceptor synaptic integrity in early diabetic retinopathy. *Invest Ophthalmol Vis Sci.* 2023;64(14):40.
https://doi.org/10.1167/iovs.64.14.40

Purpose. Diabetic retinopathy (DR) is a leading cause of blindness in working-age adults characterized by retinal dysfunction and neurovascular degeneration. We previously reported that deletion of X-box binding protein 1 (XBP1) leads to accelerated retinal neurodegeneration in diabetes; however, the mechanisms remain elusive. The goal of this study is to determine the role of XBP1 in the regulation of photoreceptor synaptic integrity in early DR.

Methods. Diabetes was induced by streptozotocin in retina-specific XBP1 conditional knockout (cKO) or wild-type (WT) mice to generate diabetic cKO (cKO/DM) or WT/DM mice for comparison with nondiabetic cKO (cKO/NDM) and WT/NDM mice. Retinal morphology, structure, and function were assessed by immunohistochemistry, optical coherence tomography, and electroretinogram (ERG) after 3 months of diabetes. The synapses between photoreceptors and bipolar cells were examined by confocal microscopy, and synaptic integrity was quantified using the QUANTOS algorithm.

Results. We found a thinning of the outer nuclear layer and a decline in the b-wave amplitude in dark- and light-adapted ERG in cKO/DM mice compared to all other groups. In line with these changes, cKO mice showed increased loss of synaptic integrity compared to WT mice, regardless of diabetes status. In searching for candidate molecules responsible for the loss of photoreceptor synaptic integrity in diabetic and XBP1-deficient retinas, we found decreased mRNA and protein levels of DLG4/PSD-95 in cKO/DM retina compared to WT/DM.

Conclusions. These findings suggest that XBP1 is a crucial regulator in maintaining synaptic integrity and retinal function, possibly through regulation of synaptic scaffold proteins.

Keywords: diabetic retinopathy, X-box binding protein 1, retinal function, photoreceptors, synaptic integrity

Diabetic retinopathy (DR) is a leading cause of blindness in working-age adults and is characterized by retinal dysfunction, neurovascular degeneration, and advanced retinal pathologies such as retinal neovascularization and fibrosis.[1,2] Although the mechanisms leading to vision loss are complex, protein dyshomeostasis in the endoplasmic reticulum (ER) has been identified as a contributing factor.[3–5] In response to ER stress, cells activate the unfolded protein response (UPR) in an attempt to restore homeostasis. The primary effectors of the UPR, activating transcription factor 6 (ATF6), PKR-like endoplasmic reticulum kinase (PERK), and inositol requiring enzyme 1 (IRE1), mediate complex pathways to increase ER folding capacity, decrease protein translation, and increase mRNA or protein degradation through the regulated Ire1-dependent decay (RIDD) or ER-associated degradation (ERAD).[6,7] As such, the UPR pathways are considered an important adaptive mechanism that allows organisms and cells to survive mild or temporary stress conditions, such as in the preclinical or early stages of human disease.[8–10] However, if homeostasis cannot be restored, is too severe, or persists for too long, cell death pathways may be activated by the UPR.[11–13] In this scenario, dysregulated UPR signaling may contribute to disease development and progression. Therefore, understanding the roles of UPR pathways in retinal cells at various stages of DR could provide insights into the mechanisms of DR pathogenesis.

A critical transcription factor of the UPR within the IRE1 pathway is X-box binding protein 1 (XBP1).[14] Upon ER stress, XBP1 is activated through unconventional splicing of XBP1 mRNA by the endoribonuclease domain of IRE1.[15] The splicing product, spliced XBP1 (XBP1s), encodes an active transcription factor that not only upregulates genes of ER chaperones and foldases to restore ER homeostasis but also regulates a myriad of genes involved in calcium signaling, mitochondrial function, autophagy, and lipid and glucose metabolism.[6,16–18] In fact, the IRE1/XBP1 pathway is the only

Investigative Ophthalmology & Visual Science

conserved UPR branch from yeast to human.[19,20] Previously, we have shown that conditional knockout (cKO) of XBP1 in retinal neurons exacerbates and accelerates retinal neurodegeneration under conditions of diabetes or aging.[10,21] The associated decline of retinal function and morphologic defects, including ERG b-wave amplitude decrease and loss of ribbon synapses, is significantly greater after 5 months of diabetes, or 1 year of age, in mice lacking XBP1 in the retina.[10,21] These findings suggest a protective role of XBP1 in retinal neuronal function and maintenance in stress or disease conditions such as aging or diabetes; however, the mechanisms remain elusive.

Photoreceptors are the most abundant and metabolically active retinal neurons responsible for phototransduction.[22] Emerging evidence suggests that diabetes-induced alterations in photoreceptor function and structure contribute to DR pathogenesis.[23] In Akita mice, a genetic model of type 1 diabetes, reduced photoreceptor ribbons and postsynaptic boutons were observed after 9 months of diabetes.[24] Using a streptozotocin (STZ)–diabetes model, we found a loss of photoreceptor synapses in retina-specific XBP1 cKO mice but not in wild-type (WT) mice after 5 months of diabetes.[21] However, the early changes in retinal synapses have not been studied. We hypothesize that damage to synaptic integrity may occur prior to the loss of synapses in diabetic retinas. In this study, we test this hypothesis by investigating retinal function in conjunction with photoreceptor synaptic integrity evaluated using the QUANTOS (QUalitative and quantitative ANalysis using Bayes Theorem Optimized for Synapse evaluation) algorithm in retina-specific XBP1 cKO and WT mice after 3 months of diabetes.

Methods

Animals

Generation of retina-specific XBP1 cKO mice was described elsewhere.[10] To induce diabetes, 9-week-old mice were given five consecutive intraperitoneal injections of streptozotocin (50 mg/kg/d; Sigma-Aldrich, St. Louis, MO, USA) or vehicle as control. Consistent blood glucose levels greater than 250 mg/dL was considered diabetic. Mice with 3 months of diabetes (but aged 5–6 months) were then compared to nondiabetic mice aged 5 to 6 months. Animal procedures were approved by the Institutional Animal Care and Use Committees at the University at Buffalo and in accordance with the guidelines of the ARVO statements for the "Use of Animals in Ophthalmic and Vision Research."

Electroretinography

A Diagnosys Espion ColorDome system and software (Diagnosys LLC, Lowell, MA, USA) was used to perform all electroretinograms as described previously.[10,21] For light-adapted ERGs, we used five flashes of 10 cd·s/m^2 (under a background of 5 cd·s/m^2) and 4-ms duration at 1 Hz. For dark-adapted ERGs, four series of three identical stimuli of light of 4-ms duration, with increasing luminance of −2.4, −1.2, 0.0, and 1.4 log(cd·s/m^2), were used with a delay of 15–60 seconds between each stimulus and each series of stimuli.

Immunofluorescence Staining

Immunofluorescence staining was performed on 12-µm (for QUANTOS and PSD-95/Ribeye labeling) and 20-µm (for GABA and SCGN labeling) retinal cryosections as described in our publications.[10,21] For QUANTOS labeling, antigen retrieval was performed with 0.1 M sodium citrate pH 6.0 at 100°C for 15 minutes. After blocking, sections were incubated with primary antibodies including anti-GABA (PC213L, 1:800, Millipore Sigma, St. Louis, Missouri, USA), anti-Ribeye (anti-ctbp2, 612044, 1:600 for QUANTOS, BD Biosciences, Franklin Lakes, New Jersey, USA; anti-Ribeye, 192 003, 1:600 for PSD-95 colabeling, Synaptic Systems, Göettingen, Germany), anti-mGluR6 (AGC-026, 1:600, Alomone, Jerusalem, Israel), and anti-PSD95 (MA1046, 1:600, ThermoFisher, Waltham, Massachusetts, USA) antibodies, followed by secondary antibodies (A11001, T6391, A11015, at 1:800, Invitrogen, Carlsbad, CA, USA). Confocal images were captured in the mid-peripheral region of the retinas with a Leica SP8 confocal microscope (Leica Biosystems, Deer Park, IL, USA) using a 63× oil immersion objective, 1024 × 1024 image size, and a z-interval of 0.30 µm. Cell bodies positive for SCGN or GABA were counted manually by two independent observers blind to genotype and diabetic condition. Counts were made across the entire field. For each animal, three to five images used and the numbers were averaged. The reported *n* values indicate number of animals.

QUANTOS Algorithm

The QUANTOS algorithm was implemented using open-source software (https://github.com/matsutakehoyo/QUANTOS) following a published protocol.[25] To train the algorithm, confocal images of 12-µm retinal cryosections labeled for Ribeye and mGluR6 from five individual WT mice were used. Five consecutive images from the confocal z-stack were selected from the interior of the z-axis to avoid edge anomalies or sectioning artifacts. For each mouse retina, three independent areas were included. Areas designated "OPL" (i.e., Ideal Synapse) or "outside-OPL" (i.e., Ideal Noise) were manually selected. Identical procedures were applied for analysis of images from all mice. Statistical analyses of QUANTOS scores were performed using the Fasano–Franceschini test, a nonparametric two-dimensional implementation of the Kolmogorov–Smirnov test, to determine whether the distributions of scores differ between groups.

Quantitative RT-PCR

Total RNA was extracted using TRIzol (Invitrogen) from mouse retinas, and cDNA was synthesized using the Bio-Rad (Hercules, CA, USA) iScript cDNA kit.[10] Quantitative RT-PCR was performed with Bio-Rad iQ SYBR Green Supermix with primers specific for mouse Dlg4/PSD95 (forward: 5′-ACGAGAGTGGTCAAGGTTAAAG-3′; reverse: 5′-GGGAGGAGACAAAGTGGTAATC-3′) and mouse β-actin (forward: 5′-GACAGGATGCAGAAGGAGATTAC-3′; reverse: 5′- TCAGTAACAGTCCGCCTAGAA-3′).

Western Blot Analysis

Proteins were extracted from mouse retinas with radio immune precipitation assay buffer containing protease inhibitor mixture, phenylmethylsulfonyl fluoride (PMSF), and sodium orthovanadate (Santa Cruz Biotechnology, Santa Cruz, CA, USA). Protein samples were resolved by a 12% SDS-PAGE gel and blotted with anti–PSD-95 (MA1-046, 1:1000, Invitrogen) and anti–β-actin (ab8226, 1:8000, Abcam,

Cambridge, MA, USA) antibodies. After incubation with horseradish peroxidase–conjugated secondary antibodies, membranes were visualized with Clarity Substrate system (Bio-Rad) on a Chemi-Doc MP Imaging device (Bio-Rad) and quantified by densitometry.

Optical Coherence Tomography

Optical coherence tomography (OCT) was performed in anesthetized mice with pupils dilated using a Micron III system and an Image-guided OCT2 device (Phoenix Technologies, Pleasanton, CA, USA). Retinal thickness measurements were performed manually by two independent observers blind to genotype and diabetic condition. Whole retina thickness was measured from the inner edge of the ganglion cell layer (GCL) to the outer edge of the outer nuclear layer (ONL). Inner retina thickness was measured from the inner edge of GCL through the outer plexiform layer.

Statistical Analyses

Statistical analyses were performed using one-way ANOVA for comparisons of three or more groups. All quantitative data were expressed as mean ± SD. Statistical differences were considered significant at a P value of less than 0.05.

Results

Decrease in b-Wave Amplitude of Dark- and Light-Adapted ERG in Diabetic cKO Mice

Previously, we found that after 5 months of diabetes, XBP1 cKO mice showed a significant reduction in both light- and dark-adapted ERG b-waves.[21] Herein, we determined to what extent, if any, retinal function declines at an earlier time point after diabetes. As shown in Figure 1A, cKO/diabetic mice (DM) demonstrated a significant reduction in dark-adapted ERG b-wave across a series of four flashes of increasing intensity compared to all other groups. There was a small and nonsignificant reduction in the b-wave responses in WT/DM mice compared to WT/nondiabetic mice (NDM) controls. Further, cKO/NDM mice aged 5 to 6 months had a-wave and b-wave responses indistinguishable from WT/NDM mice, consistent with our previous results.[10] In addition, we found no decrease in dark-adapted ERG a-wave amplitudes in either WT/DM or cKO/DM mice under diabetic conditions. In light-adapted ERGs, a-wave responses for all groups were indistinguishable from each other (Fig. 1B). Similar to dark-adapted ERG b-wave responses, light-adapted ERG b-wave amplitude was significantly reduced in cKO/DM mice compared to all other groups (Fig. 1B). A modest and nonsignificant decline in light-adapted ERG b-wave amplitude was observed in WT/DM mice (Fig. 1B). Light-adapted ERG b-wave responses in cKO/NDM mice were indistinguishable from WT/NDM mice, again confirming our previous results in adult XBP1 cKO mice.[10]

Thinning of the Retinal Outer Nuclear Layer in Diabetic cKO Mice

To determine if neurodegeneration occurs after 3 months of diabetes, we performed OCT on cKO/DM and WT/DM mice and age-matched NDM mice. Our results showed no significant change in total retinal thickness for any group, despite a trend of a thinner retina in cKO/DM mice (Fig. 2). In addition, the inner retinal thickness, measured from the GCL through the outer plexiform layer (OPL), was unchanged in any group. In contrast, there was a significant reduction in the ONL thickness in cKO/DM mice compared to all other groups in both inferior and superior retina (Fig. 2). The trend in retinal thinning in cKO/DM mice is likely attributed to the

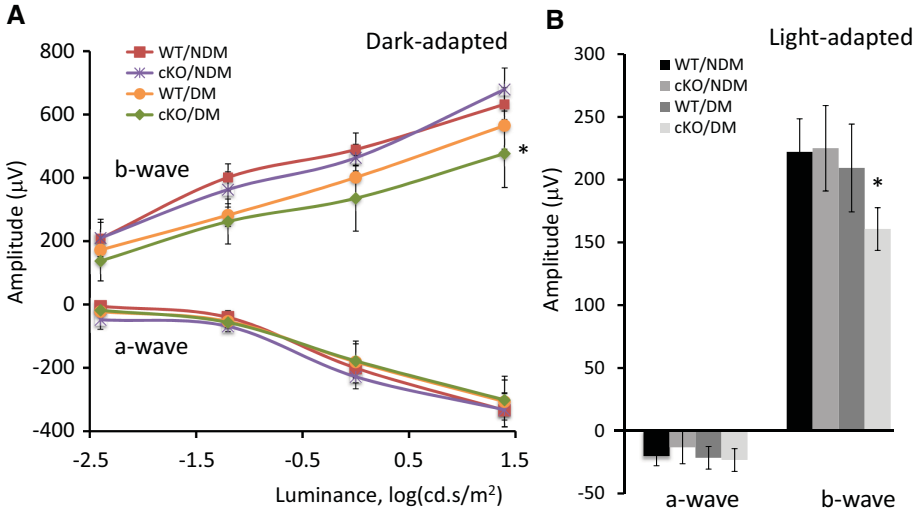

Figure 1. Reduced retinal function in cKO/DM mice. Dark- and light-adapted ERGs were performed in WT and cKO mice with or without diabetes. (**A**) Graph depicts the a- and b-wave amplitudes of dark-adapted ERG in WT/NDM ($n = 5$), cKO/NDM ($n = 3$), WT/DM ($n = 7$), and cKO/DM ($n = 7$) mice. A significant decrease in b-wave amplitude was observed in cKO/DM mice compared to WT/NDM, cKO/NDM, and WT/DM mice. *$P < 0.05$, one-way ANOVA. (**B**) Graph depicts the a- and b-wave amplitudes of light-adapted ERGs in WT/NDM ($n = 6$), cKO/NDM ($n = 3$), WT/DM ($n = 8$), and cKO/DM ($n = 6$) mice with a significant decrease in b-wave amplitude for cKO/DM mice compared to all other groups. *$P < 0.05$, one-way ANOVA with Tukey post hoc test.

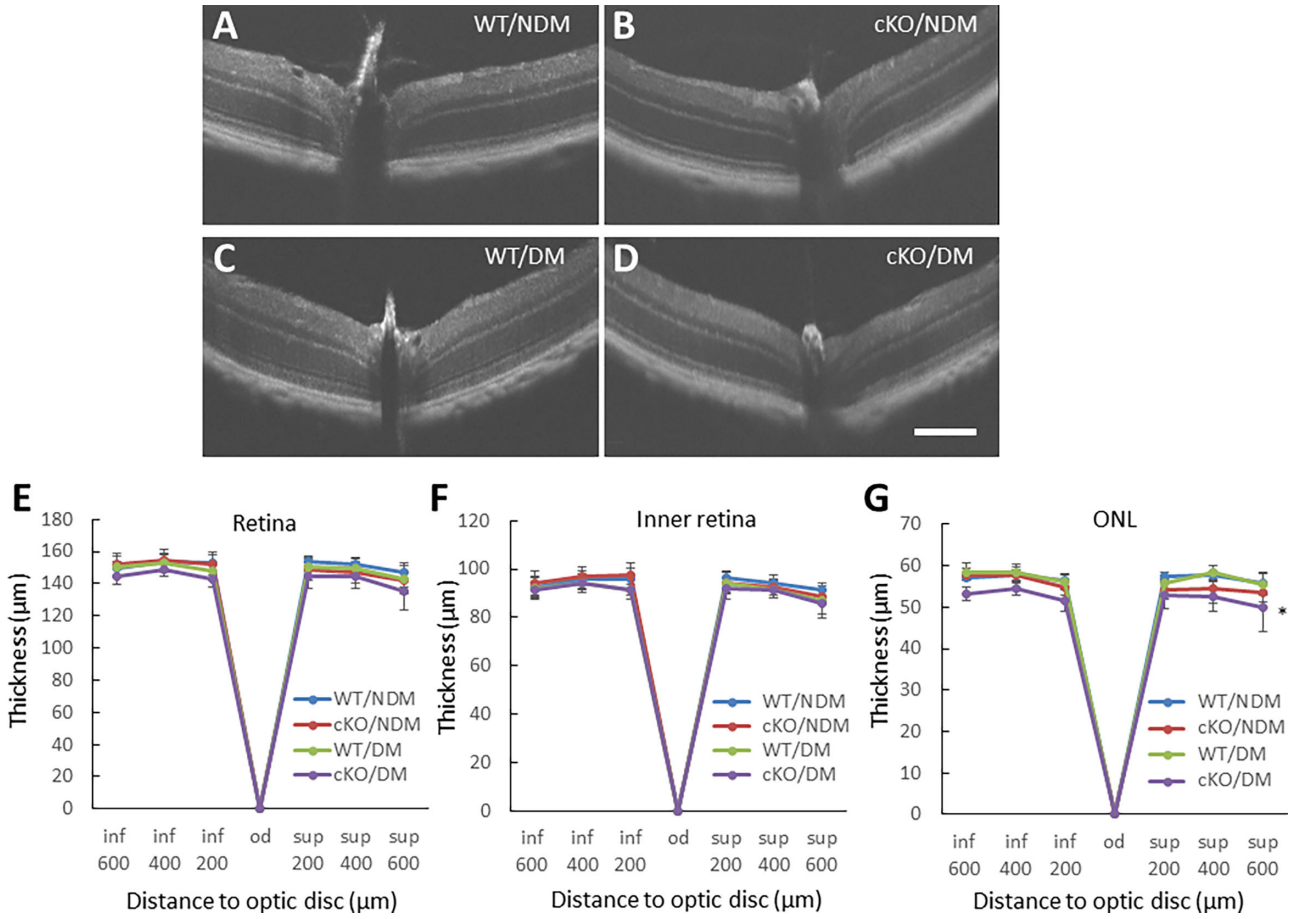

Figure 2. Thinning of retinal ONL in cKO/DM mice. OCT was performed in WT and cKO mice with or without diabetes. (**A–D**) Representative images of OCT in each group of mice. (**E–G**) Quantifications of thicknesses of the whole retina (**E**), inner retina (**F**), and ONL (**G**). A small and nonsignificant decrease in ONL thickness in WT/DM ($n = 6$) mice compared to WT/NDM ($n = 5$) mice and a significant decrease in ONL thickness in cKO/DM mice ($n = 5$) compared to WT/NDM, cKO/NDM ($n = 6$), and WT/DM mice were observed. *$P < 0.05$, one-way ANOVA with Tukey post hoc test.

significant reduction of ONL thickness. These results suggest that by 3 months of diabetes, retinal ONL neurodegeneration has begun in cKO/DM mice.

No Change in Cone Bipolar Cell Number in Diabetic cKO Retina

To determine if the decline in light-adapted ERG b-waves in the cKO/DM mice is associated with cone bipolar cell loss, we examined the morphology and number of cone bipolar cells in retinal sections with immunostaining for secretagogin (SCGN). SCGN labels cone bipolar cell bodies in the inner nuclear layer (INL), dendrites in the OPL, and terminals in the inner plexiform layer (IPL) (Fig. 3). We found no qualitative difference in SCGN-positive dendrites or terminals in cKO or WT mice regardless of diabetic conditions. Quantification of SCGN-positive cell bodies revealed no significant change in cone bipolar cell number in cKO/NDM mice compared to WT/NDM mice or in WT/DM mice compared to WT/NDM mice (Fig. 3). A slight trend for fewer cone bipolar cells was observed in cKO/DM and cKO/NDM mice compared to WT/DM and WT/NDM mice, although it did not approach significance (Fig. 3). Thus, the decrease in light-adapted ERG b-wave in the cKO/DM mice was unlikely to be caused by changes in, or loss of, cone bipolar cells at this stage.

Significant Decrease in GABAErgic Amacrine Cells in Diabetic cKO Mice

To further characterize the early stage retinal neurodegeneration in diabetic mice, we examined GABAergic amacrine cells in retinal sections labeled for gamma-aminobutyric acid (GABA). As shown in Figure 4, the immunolabeling revealed an overall distribution of GABA-positive cells in the INL and the GCL. Quantitative analysis revealed a significant decrease in total GABA-positive cells in cKO/DM mice compared to WT/DM mice (Fig. 4). Moreover, there was a nonsignificant decrease in total GABA-positive cells in cKO/NDM mice and in WT/DM mice compared to WT/NDM mice (Fig. 4). We further examined GABA-positive cells within the INL or the GCL. We found a significant decrease in GABA-positive cells in the INL of cKO/DM mice compared to other groups (Fig. 4). Interestingly, despite a trend of fewer GABA-positive cells in the GCL of cKO/DM mice, the difference was not significant. Thus, the significant decrease in total GABA-positive cells in the cKO/DM mice can be primarily attributed to the loss of GABAergic amacrine cells in the INL.

Investigative Ophthalmology & Visual Science

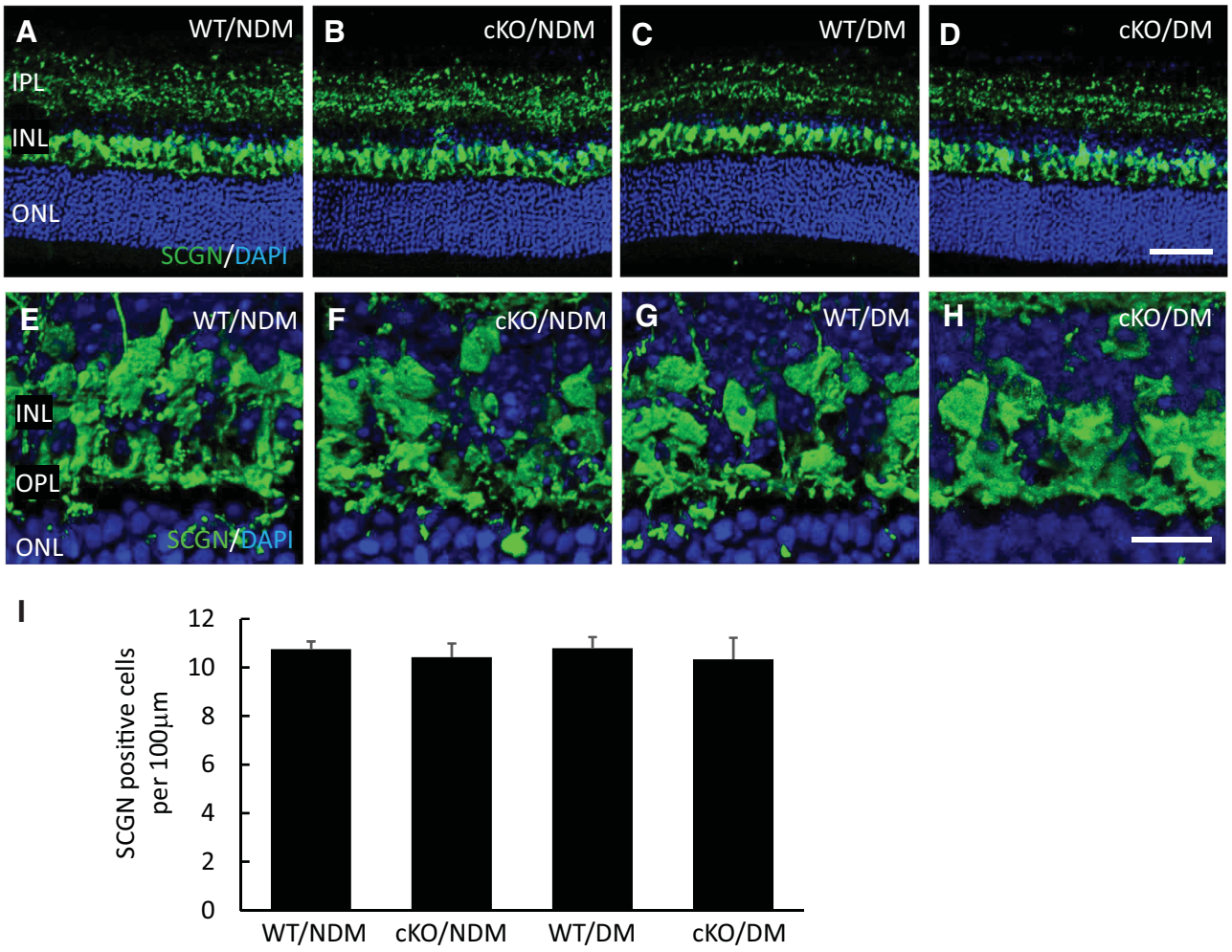

Figure 3. XBP1 deletion does not affect cone bipolar cell morphology. (**A–D**) Representative confocal images of retinal cryosections with immunofluorescence staining for SCGN (*green*) to label cone bipolar cell bodies in the INL and their dendrites and presynaptic terminals in the OPL and IPL, respectively. Nuclei were stained with DAPI (*blue*). *Scale bar*: 50 µm. (**E–H**) Higher-magnification images of cone bipolar cell bodies and dendrites in the INL and OPL. *Scale bar*: 20 µm. (**I**) Quantification of SCGN-positive cell bodies in the INL reveals no difference in cone bipolar cell numbers across the groups. $n = 4$ mice in each group. One-way ANOVA with Tukey post hoc test.

QUANTOS Algorithm Evaluates the Integrity of Photoreceptor Ribbon Synapses

Our morphologic analyses revealed either nonexistent or relatively mild degenerative changes in retinal thickness or neuronal numbers in 3-month diabetic cKO and WT mice, despite a significant functional deficit in light- and dark-adapted ERG b-waves in the cKO/DM mice. To determine the mechanism of the functional decline, we examined the synapses between photoreceptors and bipolar cells using immunohistochemistry for pre- and postsynaptic ribbon synapse markers. Double labeling with antibodies against the presynaptic marker Ribeye and against the postsynaptic marker mGluR6 revealed robust, highly specific labeling with the ONL (Fig. 5), in addition to labeling of cell bodies in the INL and synapses in the IPL for Ribeye (Fig. 5 and Supplementary Fig. S1). Close examination of three-dimensional, space-filling confocal projections at high resolution failed to reveal consistent, clear qualitative differences between groups in appearance or organization, even though individual synapses could clearly be observed at high resolution (Supplementary Fig. S1). To examine the ribbon synapses objectively and in greater detail, we used the QUANTOS algorithm to compare multiple features of the appearance of each synapse to the training data from age-matched WT/NDM mice.[25] The WT mouse retinas used to train the QUANTOS algorithm were out-of-sample to the data presented here.

The output of QUANTOS is two scores representing the similarity of each individual prospective synapse in the ONL to the ideal training data synapse, as quantified by QUANTOS using the training data across a multitude of attributes extracted from the images.[25] We found that graphs depicting these scores for each group evaluated by QUANTOS revealed a cluster of data points that appeared similarly spread along each axis (Fig. 6). When graphed in this way, each point represented a single synapse using a score for how similar that synapse was across all parameters to intact synapses (x-axis) and to degenerative synapses (y-axis) from the training data, with increasing similarity to the right and bottom of the graph, respectively. Thus, points further to the right and further toward the bottom of the distribution represented synapses most similar to the ideal, intact training synapse in adult WT/NDM mice. In contrast, points to the left and

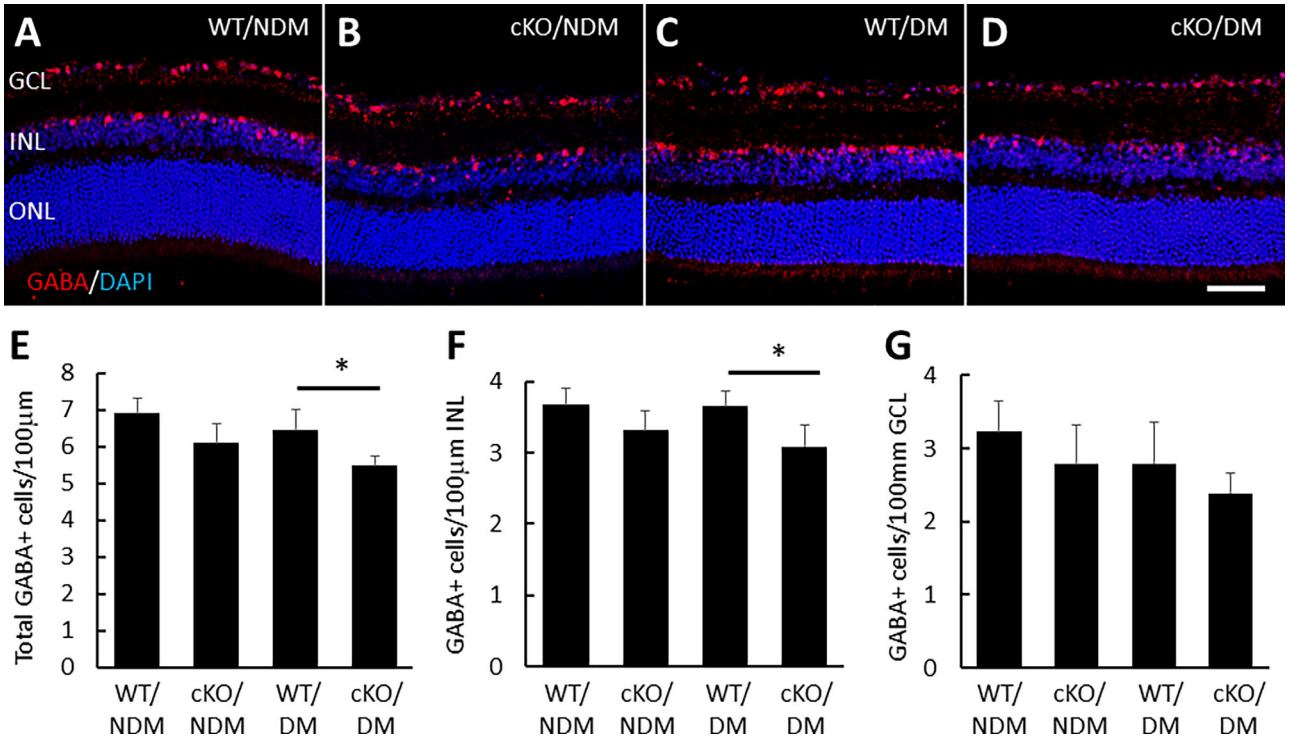

Figure 4. Decreased number of GABAergic amacrine cells in cKO/DM mice. (**A–D**) Representative confocal images of retinal cryosections with immunofluorescence staining for gamma-aminobutyric acid (GABA, *red*) to label GABAergic amacrine cells and their processes in the INL and GCL. Nuclei were stained with DAPI (*blue*). *Scale bar*: 50 µm. (**E**) Quantification of GABA-positive cell bodies in the INL and GCL reveals a nonsignificant trend for fewer GABAergic amacrine cells in cKO/NDM retinas compared to WT/NDM retinas (**E–G**). Under diabetic conditions, there was a significant reduction in GABA-positive cells in cKO/DM mice compared to WT/DM mice in total number of cells (**E**) and within the INL (**F**). *$P < 0.05$. $n = 4$ mice in each group. One-way ANOVA with Tukey post hoc test.

toward the top of the distribution represented synapses that varied from the ideal, intact training synapse and appeared more similar to degenerative synapses from the training data by this measure (Fig. 6).

Although there was substantial overlap in the distributions of the QUANTOS scores for all groups, we found a consistent and significant trend. We found that the overall distribution of scores for cKO/NDM mice was significantly shifted up and to the left of the distribution for WT/NDM mice ($P < 2.2e-16$), indicating a shift in the distribution of QUANTOS scores for synapses in XBP1 cKO/NDM mice away from ideal, intact synapses defined in WT/NDM mice and toward degenerative synapses (Fig. 6A). Similarly, there was a significant shift toward more degenerative synapses (up and to the left) in the distribution of WT/DM mice compared to WT/NDM mice ($P = 7.75e-12$) (Fig. 6B). Further, we found a significant degenerative shift in the distribution of synapse scores for cKO/DM mice compared to cKO/NDM ($P = 0.00504$) and to WT/DM mice ($P = 8.68e-06$) (Figs. 6C, 6D). These data indicate that the cKO/DM mice had the greatest proportion of synapses that appeared degenerative by this measure than all other groups. These data again suggest retinal neurodegeneration evidenced by reduced synaptic integrity had progressed in WT/DM mice after 3 months of diabetes and, to a greater extent, in cKO mice/DM with this duration of diabetes.

Potential Mechanisms for Synaptic Degeneration in Diabetic cKO Mice

To determine a mechanism for the loss of synaptic integrity in the cKO mice, we initiated a search for changes in proteins potentially involved in the structure and function of photoreceptor ribbon synapses. We found a significant reduction in the mRNA level of Dlg4, which encodes a scaffolding protein, PSD-95, in cKO/DM mice compared to WT/DM mice (Fig. 7). No difference was observed between WT/DM and WT/NDM retinas. We did observe a trend of a lower level of PSD-95 mRNA in cKO/NDM retina compared to WT/NDM retina, suggesting that XBP1 may regulate PSD-95 expression in the absence of ER stress or disease conditions. Western blot analysis confirmed a reduction in PSD-95 protein in diabetic cKO retina (Fig. 7). Additionally, immunohistochemistry (IHC) for PSD-95 and Ribeye supports the reduction in PSD-95 in cKO/DM retina (Fig. 7). These data suggest the combined effects of diabetes and XBP1 deficiency in retina results in a significant decline in PSD-95. The decrease in this critical scaffolding protein at the ribbon synapse may contribute to both the observed functional deficits in the ERG as well as the loss of synaptic integrity revealed with the QUANTOS algorithm in the cKO mice.

Discussion

The long time course of DR and multifaceted pathogenic factors, such as metabolic and oxidative stress, suggest a plausible role of cellular stress response in the development of retinal neurodegeneration and vision loss. Previously, we reported that retina-specific deletion of XBP1, a critical transcription factor that coordinates cellular stress response, led to accelerated age-related retinal neurodegeneration and exacerbated retinal morphologic and functional deficits in mice after 5 months of diabetes.[21] To uncover the initial events and mechanisms of retinal neurodegeneration

Investigative Ophthalmology & Visual Science

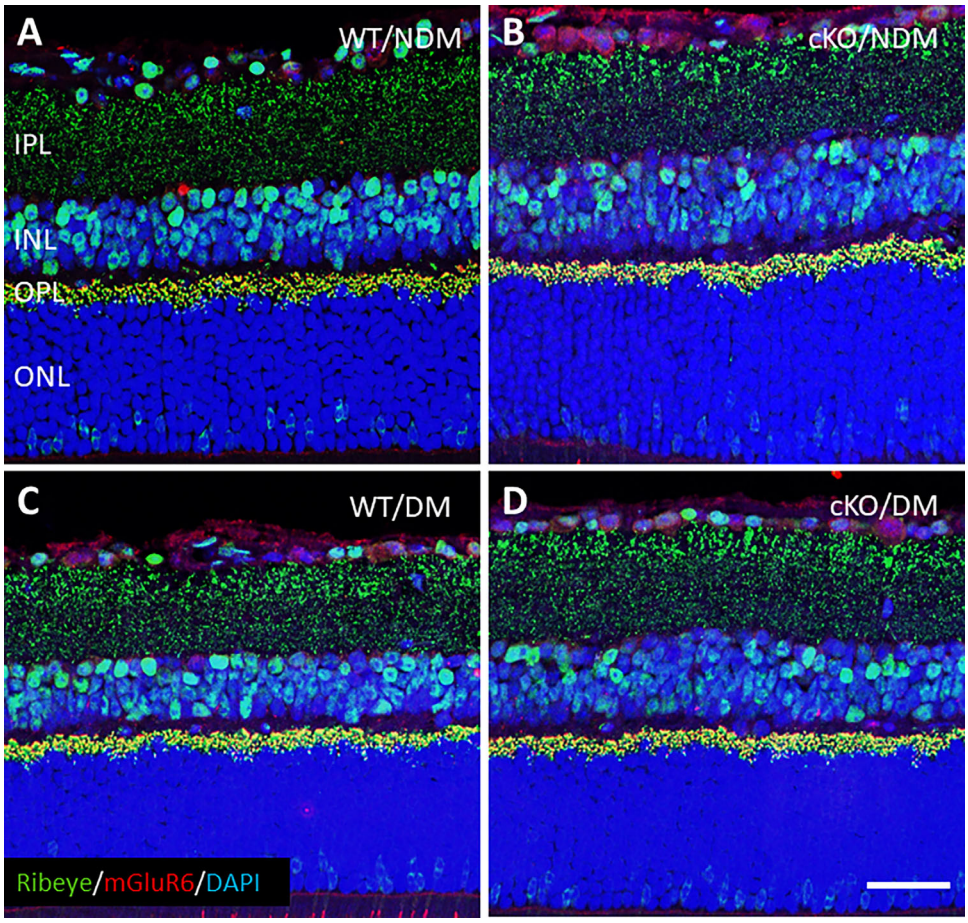

Figure 5. Confocal microscopy of ribbon synapses labeled with Ribeye and mGluR6 in mouse retinas. Cryosections (12 µm thick) of mouse retinas were stained with antibodies against metabotropic glutamate receptor 6 (mGluR6, *red*) and Ribeye (*green*) to label the presynaptic (Ribeye) and postsynaptic (mGluR6) components of ribbon synapses between photoreceptors and bipolar cells in the OPL. Ribeye also extensively labeled synapses within the IPL. Nuclei were stained with DAPI (*blue*). (**A–D**) Representative confocal images from five mice per group. Each image is a projection of confocal scans taken from five consecutive focal planes. *Scale bar*: 50 µm.

associated with XBP1 deficiency and diabetes, we examined the cKO/DM mice with 3 months of diabetes to discern the early changes. We found a significant reduction in both light- and dark-adapted ERG b-wave amplitudes in cKO/DM mice but not in WT/DM mice, supporting that loss of XBP1 accelerates retinal neurodegeneration in diabetes. Consistent with the functional changes, a significant thinning of the ONL and a small, but significant, decrease in GABAergic amacrine cells within the INL was observed in cKO/DM mice. In contrast, we found no difference in cone bipolar cells across all groups, suggesting that cone bipolar cell survival is not affected by loss of XBP1 or by diabetes at this stage.

The ERG b-wave is primarily attributed to bipolar cell responses. Our data show that there was no difference in bipolar cell number or morphology, indicating that the functional deficit in cKO/DM mice was not likely caused by loss of bipolar cells. Previously, we reported that the number of photoreceptor ribbon synapses was reduced in cKO/DM mice after 5 months of diabetes.[10] We hypothesized that there may be disruption of the synaptic integrity prior to the loss of synapses. To test this hypothesis, we carried out a quantitative analysis of synaptic integrity using the QUANTOS algorithm.[25] This method allowed us to assess the synaptic integrity of individual ribbon synapses in great detail by evaluating the likelihood that each pairing of Ribeye and mGluR6 present in the confocal image stack represented an intact synapse or a degenerative synapse. Thus, the distribution of all evaluated synapses provided a population-level assessment of synaptic integrity.

Our results showed that the overall distributions of the synapses overlapped substantially across the groups. However, the distribution of QUANTOS scores of synaptic integrity shifted up and to the left significantly toward more degenerative synapses under diabetic conditions and due to the loss of XBP1 in the retina. Thus, changes at the ribbon synapse that were difficult or impossible to detect by standard qualitative examination of IHC were nonetheless occurring at 3 months of diabetes, and these changes were exacerbated by the loss of XBP1. Moreover, cKO/NDM mice demonstrated reduced synaptic integrity compared to WT/NDM mice, indicating that the initial stages of neurodegeneration had begun in the cKO mice prior to 6 months of age; interestingly, the manifestation of structural and functional deficits was not observed in these mice until well after 8 months of age using standard immunohistochemistry techniques and microscopy.[10] Importantly, we found a loss of synaptic integrity of ribbon synapses in cKO/DM mice

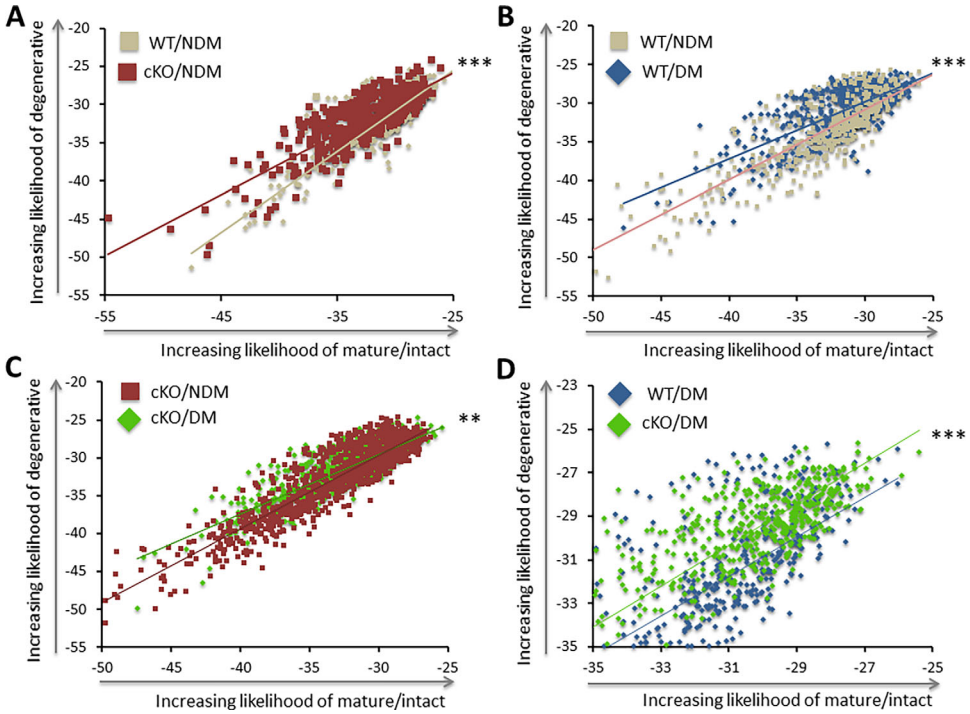

Figure 6. Reduced integrity of ribbon synapses in WT/DM, cKO/NDM, and cKO/DM mice quantified by the QUANTOS algorithm. Graphs depict QUANTOS Bayes scores of individual synapses. (**A**) Combined QUANTOS Bayes scores for synapses from WT/NDM and cKO/NDM mice. The distribution of scores for XBP1 cKO/NDM mice is significantly shifted up and to the left when compared to WT/NDM mice. (**B**) The distribution of scores for WT/DM mice is significantly shifted up and to the left when compared to WT/NDM mice. (**C**) The distribution of scores for cKO/DM mice is significantly shifted up and to the left when compared to cKO/NDM mice. (**D**) Graph shows a significant shift up and to the left for cKO/DM mice compared to WT/DM mice. *Lines* represent linear trendlines. $n = 5$ mice for each group. $^{**}P < 0.01$; $^{***}P < 0.0001$, Fasano–Franceschini test.

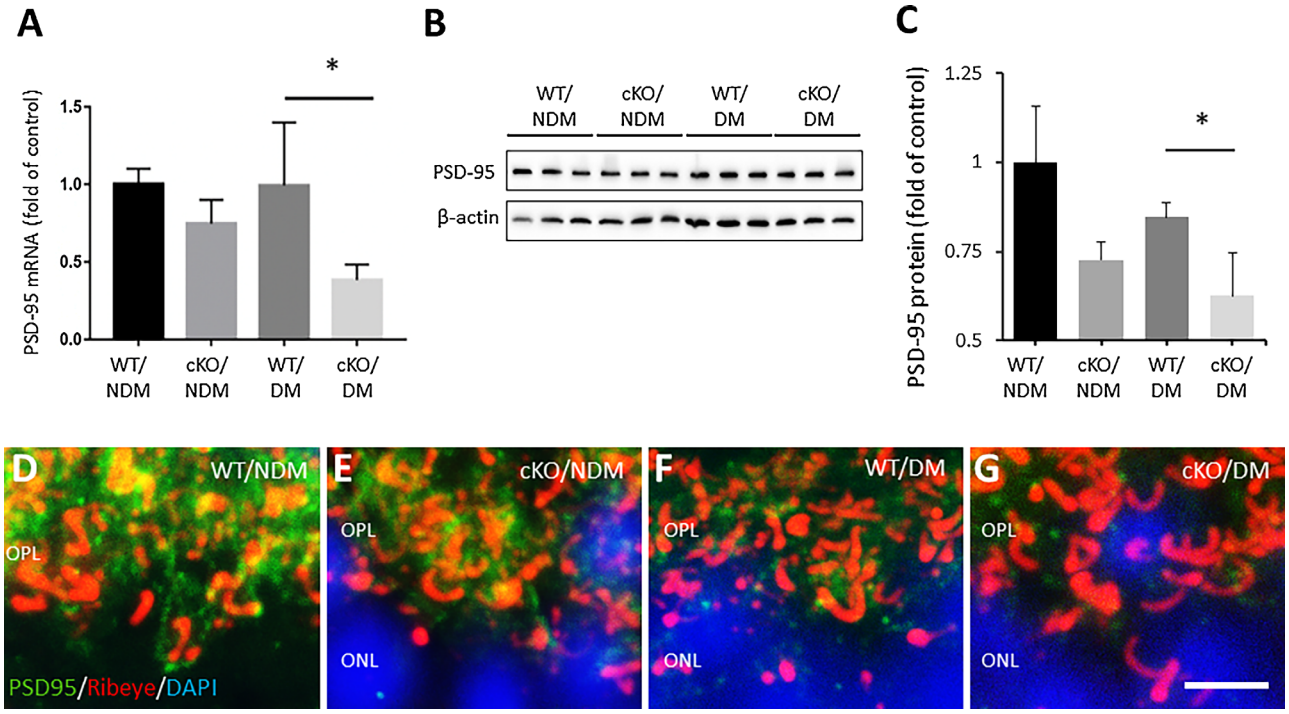

Figure 7. Reduced levels of PSD-95 mRNA and protein in cKO/DM mice. (**A**) mRNA levels of Dlg4/PSD-95 in the retinas were measured by quantitative RT-PCR with β-actin as an internal control. $n = 3$ mice for each group. $^{*}P < 0.05$. (**B**, **C**) Western blot analysis of PSD-95 and quantitation with densitometry. $n = 3$ mice for each group. $^{*}P < 0.05$. (**D–G**) Confocal images of retinal cryosections with double immunofluorescence labeling for PSD-95 (*green*) and Ribeye (*red*) showing a reduction in PSD-95 in cKO/DM retina. Nuclei were stained with DAPI (*blue*). *Scale bar*: 5 µm. One-way ANOVA with Tukey post hoc test.

Investigative Ophthalmology & Visual Science

compared to all other groups, which correlated well with the functional decline in the ERG b-wave amplitude. Moreover, we found a loss of synaptic integrity in WT/DM mice compared to WT/NDM mice, although we saw only a trend for functional decline in the ERG between these groups, indicating that 3 months of diabetes was near the onset of significant structural and functional synaptic degeneration. This study, to our knowledge, is the first to demonstrate reduced retinal synaptic integrity that may contribute to retinal function decline in early diabetes.

The mechanisms behind the impaired synaptic integrity in XBP1 cKO and diabetic retinas are complex and understudied. A recent study showed that overexpression of XBP1s, the active form of XBP1, in the brain improved synaptic function in part through restoring the levels of several synaptic proteins and factors involved in actin cytoskeleton regulation and axonal growth.[26] In the present study, we examined the expression of PSD-95, a major synaptic protein,[27,28] in the retina. We found that both the mRNA and protein levels of PSD-95 were significantly reduced in the cKO/DM retina. In addition, increased RhoA activation was recently linked to synaptic damage in a retinal detachment model.[29,30] RhoA associates with metabotropic glutamate receptors and also regulates cytoskeletal dynamics.[31,32] It also serves as an upstream regulator of cofilin 1, a regulator of actin dynamics in spines and involved in early stage neurodegeneration through formation of cofilin/actin rods.[26,30] In the 5XFAD mouse model of Alzheimer disease, cofilin 1 is downregulated and overexpression of XBP1 restores cofilin 1 expression.[26] Thus, it is plausible that lack of XBP1 in bipolar cells and/or photoreceptors may alter synaptic architecture by reducing the levels of proteins involved in cytoskeletal dynamics and that this dysfunction leads to diminished function and degenerative appearance of ribbon synapses. This possibility needs to be further investigated in future studies.

In summary, our study shows that retinal neurodegeneration occurs in STZ-diabetic mice at approximately 3 months of diabetes and that loss of XBP1 in retinal neurons accelerates this process. Further, the synaptic integrity exists on a scale from intact to degenerative, with both diabetes and loss of XBP1 tilting the scale toward a degenerative appearance, likely due to dysregulation of synaptic proteins, resulting in functional deficits. Understanding the mechanisms of these early changes may provide new approaches for protecting retinal neurons and improving retinal function in DR.

Acknowledgments

The authors thank Leslie Ying (University at Buffalo) for her advice and discussions on QUANTOS analysis.

Supported, in part, by NIH/NEI grants EY019949, EY025061, and EY030970 (to SXZ); a research grant NGR G2019302 from the Brightfocus Foundation (to SXZ); and an unrestricted grant from Research to Prevent Blindness to the Department of Ophthalmology, the State University of New York at Buffalo.

Disclosure: **T. McLaughlin**, None; **G. Wang**, None; **A. Medina**, None; **J. Perkins**, None; **R. Nihlawi**, None; **D. Seyfried**, None; **Z. Hu**, None; **J.J. Wang**, None; **S.X. Zhang**, None

References

1. Simo R, Stitt AW, Gardner TW. Neurodegeneration in diabetic retinopathy: does it really matter? *Diabetologia*. 2018;61:1902–1912.
2. Levine SR, Sapieha P, Dutta S, Sun JK, Gardner TW. It is time for a moonshot to find "Cures" for diabetic retinal disease. *Prog Retin Eye Res*. 2022;90:101051.
3. Ma JH, Wang JJ, Zhang SX. The unfolded protein response and diabetic retinopathy. *J Diabetes Res*. 2014;2014:14.
4. Zhang SX, Sanders E, Fliesler SJ, Wang JJ. Endoplasmic reticulum stress and the unfolded protein responses in retinal degeneration. *Exp Eye Res*. 2014;125C:30–40.
5. Li J, Wang JJ, Yu Q, Wang M, Zhang SX. Endoplasmic reticulum stress is implicated in retinal inflammation and diabetic retinopathy. *FEBS Lett*. 2009;583:1521–1527.
6. McLaughlin T, Medina A, Perkins J, Yera M, Wang JJ, Zhang SX. Cellular stress signaling and the unfolded protein response in retinal degeneration: mechanisms and therapeutic implications. *Mol Neurodegener*. 2022;17:25.
7. Zhang SX, Ma JH, Bhatta M, Fliesler SJ, Wang JJ. The unfolded protein response in retinal vascular diseases: implications and therapeutic potential beyond protein folding. *Prog Retin Eye Res*. 2015;45C:111–131.
8. Li J, Wang JJ, Zhang SX. Preconditioning with endoplasmic reticulum stress mitigates retinal endothelial inflammation via activation of X-box binding protein 1. *J Biol Chem*. 2011;286:4912–4921.
9. Zhong Y, Li J, Wang JJ, et al. X-box binding protein 1 is essential for the anti-oxidant defense and cell survival in the retinal pigment epithelium. *PLoS ONE*. 2012;7:e38616.
10. McLaughlin T, Falkowski M, Park JW, et al. Loss of XBP1 accelerates age-related decline in retinal function and neurodegeneration. *Mol Neurodegener*. 2018;13:16.
11. Jing G, Wang JJ, Zhang SX. ER stress and apoptosis: a new mechanism for retinal cell death. *Exp Diabetes Res*. 2012;2012:589589.
12. Chen C, Cano M, Wang JJ, et al. Role of unfolded protein response dysregulation in oxidative injury of retinal pigment epithelial cells. *Antioxid Redox Signal*. 2014;20:2091–2106.
13. Huang C, Wang JJ, Ma JH, Jin C, Yu Q, Zhang SX. Activation of the UPR protects against cigarette smoke-induced RPE apoptosis through up-regulation of Nrf2. *J Biol Chem*. 2015;290:5367–5380.
14. Glimcher LH. XBP1: the last two decades. *Ann Rheum Dis*. 2010;69:i67–i71.
15. Yoshida H, Matsui T, Yamamoto A, Okada T, Mori K. XBP1 mRNA is induced by ATF6 and spliced by IRE1 in response to ER stress to produce a highly active transcription factor. *Cell*. 2001;107:881–891.
16. Piperi C, Adamopoulos C, Papavassiliou AG. XBP1: a pivotal transcriptional regulator of glucose and lipid metabolism. *Trends Endocrinol Metab*. 2016;27:119–122.
17. Yamamoto K, Sato T, Matsui T, et al. Transcriptional induction of mammalian ER quality control proteins is mediated by single or combined action of ATF6alpha and XBP1. *Dev Cell*. 2007;13:365–376.
18. Ma JH, Wang JJ, Li J, Pfeffer BA, Zhong Y, Zhang SX. The role of IRE-XBP1 pathway in regulation of retinal pigment epithelium tight junctions XBP1 regulates the RPE tight junctions. *Invest Ophthalmol Vis Sci*. 2016;57:5244–5252.
19. Reimold AM, Etkin A, Clauss I, et al. An essential role in liver development for transcription factor XBP-1. *Genes Dev*. 2000;14:152–157.
20. Cox JS, Walter P. A novel mechanism for regulating activity of a transcription factor that controls the unfolded protein response. *Cell*. 1996;87:391–404.
21. McLaughlin T, Siddiqi M, Wang JJ, Zhang SX. Loss of XBP1 leads to early-onset retinal neurodegeneration in a mouse model of type I diabetes. *J Clin Med*. 2019;8:906.
22. Hurley JB, Lindsay KJ, Du J. Glucose, lactate, and shuttling of metabolites in vertebrate retinas. *J Neurosci Res*. 2015;93:1079–1092.

23. Tonade D, Kern TS. Photoreceptor cells and RPE contribute to the development of diabetic retinopathy. *Prog Retin Eye Res*. 2021;83:100919.
24. Hombrebueno JR, Chen M, Penalva RG, Xu H. Loss of synaptic connectivity, particularly in second order neurons is a key feature of diabetic retinal neuropathy in the Ins2Akita mouse. *PLoS One*. 2014;9:e97970.
25. Akiba R, Matsuyama T, Tu HY, et al. Quantitative and qualitative evaluation of photoreceptor synapses in developing, degenerating and regenerating retinas. *Front Cell Neurosci*. 2019;13:16.
26. Duran-Aniotz C, Poblete N, Rivera-Krstulovic C, et al. The unfolded protein response transcription factor XBP1s ameliorates Alzheimer's disease by improving synaptic function and proteostasis. *Mol Ther*. 2023;31:2240–2256.
27. Blackmon SM, Peng YW, Hao Y, et al. Early loss of synaptic protein PSD-95 from rod terminals of rhodopsin P347L transgenic porcine retina. *Brain Res*. 2000;885:53–61.
28. Koulen P, Fletcher EL, Craven SE, Bredt DS, Wässle H. Immunocytochemical localization of the postsynaptic density protein PSD-95 in the mammalian retina. *J Neurosci*. 1998;18:10136–10149.
29. Wang J, Zarbin M, Sugino I, Whitehead I, Townes-Anderson E. RhoA signaling and synaptic damage occur within hours in a live pig model of CNS injury, retinal detachment. *Invest Ophthalmol Vis Sci*. 2016;57:3892–3906.
30. Wang W, Halasz E, Townes-Anderson E. Actin dynamics, regulated by RhoA-LIMK-cofilin signaling, mediates rod photoreceptor axonal retraction after retinal injury. *Invest Ophthalmol Vis Sci*. 2019;60:2274–2285.
31. Schubert V, Da Silva JS, Dotti CG. Localized recruitment and activation of RhoA underlies dendritic spine morphology in a glutamate receptor-dependent manner. *J Cell Biol*. 2006;172:453–467.
32. Schmidt SI, Blaabjerg M, Freude K, Meyer M. RhoA signaling in neurodegenerative diseases. *Cells*. 2022;11(9):1520.

Investigative Ophthalmology & Visual Science